Diffraction patterns of He atoms from the MgO(100) surface calculated by the close-coupling method

2007 J. Phys.: Condens. Matter 19 305006

(http://iopscience.iop.org/0953-8984/19/30/305006)

IOP PUBLISHING JOURNAL OF PHYSICS: CONDENSED MATTER

J. Phys.: Condens. Matter **19** (2007) 305006 (10pp) doi:10.1088/0953-8984/19/30/305006

Diffraction patterns of He atoms from the MgO(100) surface calculated by the close-coupling method

R Martínez-Casado[1,2], B Meyer[3], S Miret-Artés[2], F Traeger[1] and Ch Wöll[1]

[1] Lehrstuhl für Physikalische Chemie I, Ruhr-Universität Bochum, D-44780 Bochum, Germany
[2] Instituto de Matemáticas y Física Fundamental, Consejo Superior de Investigaciones Científicas, Serrano 123, 28006 Madrid, Spain
[3] Lehrstuhl für Theoretische Chemie, Ruhr-Universität Bochum, D-44780 Bochum, Germany

E-mail: ruth@imaff.cfmac.csic.es

Received 5 February 2007, in final form 13 March 2007
Published 13 July 2007
Online at stacks.iop.org/JPhysCM/19/305006

Abstract

An analysis of He diffraction data for the MgO(001) surface which goes beyond hard-wall eikonal approximations is presented. In a first step, a model potential, for which the form of a corrugated Morse potential is chosen, is set up using the eikonal approximation in connection with an effective corrugation function. The obtained corrugation amplitude is compared to results from density-functional theory calculations of the He–MgO interaction. In a second step, this model potential is used for close-coupling (CC) calculations of He diffraction intensities. A kinematical analysis of the system He/MgO is given. The results on the He diffraction intensities are in good agreement with the experiment.

(Some figures in this article are in colour only in the electronic version)

1. Introduction

In recent years the number of studies on oxide surfaces has largely increased and several review articles have been published [1–6]. Despite very careful investigations and optimized methods, inherent problems remain: oxides are insulating materials, for which all methods using or producing electrons are frequently hampered by artifacts due to charging or due to damage produced by impinging electrons. In some cases, the use of very low electron currents, nowadays available e.g. in channel plate low-energy electron diffraction (LEED) systems, reduces these artifacts. In other cases, for instance ZnO or TiO_2, a conduction mechanism via defects sets in and facilitates the use of scanning tunnelling microscopy (STM), LEED and other well-developed standard techniques [3]. Except for the cleavage faces of the rocksalt-type oxides, MgO, NiO and CoO [7–15], on most oxide surfaces usually a comparatively large defect density is present, which decreases the reliability of methods which cannot distinguish

between a signal from well-ordered parts of the surface and a signal from defective parts, like photoelectron spectroscopy (XPS) or thermal desorption spectroscopy (TDS). He-atom scattering is a technique which uses neutral particles of subthermal energy (10–80 meV) and, therefore, is not complicated by charging and damaging effects; see [16–18] and references therein. Additionally, the scattering cross section between He atoms and surface defects is large: point defects reveal a scattering cross section of 100 $Å^2$ and step edges appear as 10 Å wide [19]. The consequence is that nearly all the detectable signal stems from coherent scattering from the periodically ordered parts of the surface. Similarly, the scattering cross sections between He and H atoms are in the range of 10 $Å^2$ [19], resulting in sensitivity to the presence of hydroxyl groups on the surface which cannot easily be detected with LEED. Beyond structural investigations, it is possible to measure adsorbate dynamics by inelastic scattering and to obtain information on the He-surface interaction potential.

Relying on a diffraction technique, however, requires a conversion of the information gained in reciprocal space to real-space structures. This becomes especially important if an initially unknown structure or properties of molecular adsorbates are investigated. The calculations of diffraction intensities for model corrugation functions is the first step, often realized with rather simple hard-wall eikonal models [20], which has been done extensively for the example of MgO; see [7, 10, 12, 13, 18, 21]. In the case of oxide surfaces, only the eikonal methods have been applied so far, although the large corrugation of ionic crystals raises the question of the applicability of these models. Exact methods like CC [22–27] or time-dependent wave packet [26–28] calculations have been developed and applied mainly to ionic and metallic surfaces. However, these accurate methods are not passable as well, since for most oxides no reliable He-surface potentials are available.

In this work we assess the first steps towards a more realistic description of He scattering from oxide surfaces beyond the hard-wall eikonal approximation. We adopt a simple model potential for the He-surface interaction, and we analyse the He diffraction from the MgO(001) surface with the CC method. MgO(001) is the best-characterized oxide surface, for which most experimental data is available. From this data, realistic parameters for the attractive part of our model potential are extracted. To obtain reliable information on the corrugation amplitude of the potential, we first reinvestigate a previous analysis of the MgO system within the simplest form of the eikonal approximation [21]. Then the eikonal fit is refined by using an effective corrugation function which we derive from our model potential. The deduced corrugation amplitude, which in the standard eikonal analysis is interpreted geometrically as a height difference between ions in the unit cell, is compared to results from density-functional theory (DFT) calculations on the He–MgO repulsion potential. Finally, the parametrized model potential is used in CC calculations to investigate whether such a model potential is valid in an exact scattering calculation beyond the assumptions made for its derivation.

The organization of this work is as follows. In section 2, a description of the standard experimental setup is introduced. The eikonal approximation as well as the CC method are presented in section 3. The results from both methods as well as from the DFT calculations are shown in section 4. Finally, the conclusions from this work are summarized in section 5.

2. Experiment

A detailed description of the experimental apparatus is given in [29]. A nearly mono-energetic He-atom beam is diffracted from the surface in a fixed angle geometry; see figure 1. The incident and final angles, θ_i and final θ_f, measured with respect to the surface normal, obey the relationship $\theta_i + \theta_f = 90.1°$. The parallel wavevector change is given by

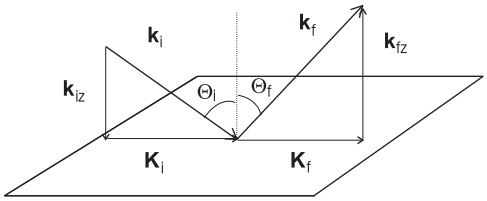

Figure 1. Geometry of the fixed angle in-plane scattering experiment and definition of symbols. $\mathbf{k}_{i,f}$ are the incident and final wavevectors, whereas $\mathbf{K}_{i,f}$ are the wavevector components parallel to the surface.

$|\Delta\mathbf{K}| = |\mathbf{k}_f| \cdot \sin\theta_f - |\mathbf{k}_i| \cdot \sin\theta_i$, where $\mathbf{k}_i$ and $\mathbf{k}_f$ are the incident and final wavevectors. For a comparison with theory, a more favourable geometry would be a fixed incident angle and a variable exit angle, which cannot be realized with this type of apparatus optimized for time-of-flight resolution. The MgO(001) surface was prepared by cleaving a $10 \times 10 \times 10$ mm^3 MgO sample *in situ* at room temperature and the quality of the surface was checked by comparing He angular distributions routinely before every experiment. The experimental data, which are theoretically analysed in this paper, have been published in [21].

3. Theory

3.1. The interaction potential model

In this work a corrugated Morse potential model (originally proposed by Armand and Manson [30]) has been used to simulate the atom–surface interaction

$$V(\mathbf{R}, z) = D\left(\frac{1}{\nu_{\mathbf{0}}}\mathrm{e}^{-2\chi[z-\xi(\mathbf{R})]} - 2\mathrm{e}^{-\chi z}\right), \tag{1}$$

where D is the well depth, χ is the stiffness parameter, $\xi(\mathbf{R})$ is the corrugation or shape function, $\mathbf{R}$ is a surface lattice vector and $\nu_{\mathbf{0}}$ is the surface average of the exponential of the corrugation function (see equation (3)). Taking into account the periodicity of the corrugation function, this potential can be more conveniently expanded in a Fourier series as

$$V(\mathbf{R}, z) = V_{\mathbf{0}}(z) + \sum_{\mathbf{G}\neq\mathbf{0}} V_{\mathbf{G}}(z)\,\mathrm{e}^{\mathrm{i}\mathbf{G}\cdot\mathbf{R}}. \tag{2}$$

The Fourier coefficients $V_{\mathbf{G}}(z)$ can be expressed as analytical functions in terms of the corrugation Fourier coefficients $\nu_{\mathbf{G}}$, which are given by

$$\nu_{\mathbf{G}} = \frac{1}{S}\int_U \mathrm{e}^{-\mathrm{i}\mathbf{G}\cdot\mathbf{R}}\,\mathrm{e}^{2\chi\xi(\mathbf{R})}\,\mathrm{d}\mathbf{R}. \tag{3}$$

This integral is carried out over the surface unit cell U of area S, with $\mathbf{G}$ being a reciprocal lattice vector. The first Fourier coefficient of the potential or bare potential is given by

$$V_{\mathbf{0}}(z) = D(\mathrm{e}^{-2\chi z} - 2\mathrm{e}^{-\chi z}). \tag{4}$$

Higher-order coefficients (with $\mathbf{G} \neq \mathbf{0}$) are responsible for the coupling in the diffraction process and are given by

$$V_{\mathbf{G}}(z) = \frac{D\nu_{\mathbf{G}}}{\nu_{\mathbf{0}}}\mathrm{e}^{-2\chi z}. \tag{5}$$

3.2. The eikonal approximation

The eikonal approximation in its most simple form [20] uses a hard corrugated wall. This method has been applied to MgO [21]. However, it is not expected to be valid for perpendicular energies similar to the well depth of the bare potential and for largely corrugated surfaces. In general, strong discrepancies with theoretical results coming from more refined methods have been reported, in particular with CC results [25, 31]. To account for the slope of the repulsive part of the potential, the method can be improved by using an effective corrugation function [25] that depends on the incident energy, E_i.

The MgO(001) surface has a square surface unit cell. The corresponding reciprocal lattice vectors are given by $\mathbf{G} = (2\pi/a)(n, m)$, where a is the surface cell lattice parameter with a value of $a = 2.98$ Å. In this work only He diffraction intensities along the MgO(001)⟨100⟩ direction have been analysed. For the corrugation function in the model potential of equation (1) we have adopted the simple form

$$\xi(x, y) = \frac{\xi_0}{2}\left(\cos\left(\frac{2\pi x}{a}\right) + \cos\left(\frac{2\pi y}{a}\right)\right), \tag{6}$$

where ξ_0 is the corrugation amplitude. The parameters for the attractive part of the potential were taken from the experimental study [21] where, from an analysis of He bound states on the MgO(001) surface, a potential well depth of $D = 12.5$ meV and a stiffness parameter of $\chi = 1.05$ Å^{-1} have been deduced. In our CC calculations, the well depth value has been kept fixed but the stiffness parameter has been changed slightly for the two incident energies analysed. A first estimate of the corrugation amplitude, ξ_0, is also provided by [21]. From a simple eikonal analysis of the diffraction intensities, using the energy-independent corrugation function equation (6) directly, a value of $\xi_0 = 0.16$ Å has been obtained.

3.3. The effective corrugation function

Equipotential surfaces can be obtained from the classical turning points of the potential, which are defined as the locus of all points such that $V(\mathbf{R}, z) = E_i$. The implicit function $z = \xi_{E_i}(\mathbf{R})$ is called the *effective corrugation function* and depends on the well depth and total energy E_i of the collision. This function reads as [25]

$$\xi_{E_i}(\mathbf{R}) = \frac{1}{\chi}\ln\left\{-\frac{D}{E_i} + \sqrt{\frac{D^2}{E_i^2} + \frac{D}{E_i}\left(1 + \sum_{\mathbf{G}\neq\mathbf{0}}\frac{v_\mathbf{G}}{v_\mathbf{0}}\,e^{i\mathbf{G}\cdot\mathbf{R}}\right)}\right\}. \tag{7}$$

For the system considered here, this function decreases monotonically over the whole range from 10 to 80 meV. This is one of the main drawbacks of the model potential equation (1). It can be overcome if the Fourier coefficients defined in equation (3) are modified at different incident energies of the atomic beam in order to obtain the correct behaviour, that is, an increase in the corrugation with E_i.

3.4. The CC formalism

Consider the elastic scattering of a structureless, non-penetrating particle (with incidence wavevector $\mathbf{k}_i$) off a statically corrugated periodic solid surface. The (parallel) momentum conservation is given by the Bragg or diffraction condition

$$\Delta\mathbf{K} = \mathbf{K}_f - \mathbf{K}_i = \mathbf{G} \tag{8}$$

and the time-independent Schrödinger equation describing this process is

$$\left(-\nabla^2 + V(\mathbf{R}, z) - \mathbf{k}_i^2\right)\Psi(\mathbf{R}, z) = 0 \tag{9}$$

written in units where $\hbar^2/2m = 1$, with m being the He atom mass [23, 27]. Due to the surface periodicity, both the interaction potential and the wavefunction can be Fourier expanded. The expansion for the former is given by equation (2), and for the latter it is

$$\Psi(\mathbf{R}, z) = \sum_{\mathbf{G}} \Psi_{\mathbf{G}}(z)\, \mathrm{e}^{\mathrm{i}(\mathbf{K}_\mathrm{i}+\mathbf{G})\cdot\mathbf{R}}. \tag{10}$$

Substituting equations (2) and (10) into equation (9), multiplying the resulting expression by $\exp[-\mathrm{i}(\mathbf{K}_\mathrm{i}+\mathbf{G})\cdot\mathbf{R}]$, and then integrating over the area of a single surface unit cell, one obtains the following set of coupled equations, namely the *CC equations*, for the diffracted waves:

$$\left(\frac{\mathrm{d}^2}{\mathrm{d}z^2} + \mathbf{k}^2_{\mathbf{G},z} - V_{\mathbf{0}}(z)\right) \Psi_{\mathbf{G}}(z) = \sum_{\mathbf{G}'\neq\mathbf{G}} V_{\mathbf{G}-\mathbf{G}'}(z)\ \Psi_{\mathbf{G}'}(z), \tag{11}$$

where $V_{\mathbf{0}}(z)$ is the laterally and thermally averaged interaction potential, and

$$\mathbf{k}^2_{\mathbf{G},z} = \mathbf{k}^2_\mathrm{i} - (\mathbf{K}_\mathrm{i} + \mathbf{G})^2 \tag{12}$$

gives the z-component kinetic energy of the **G**-diffracted wave. Equation (11) is solved with the appropriate boundary conditions [25, 27]. The square moduli of the outgoing wave amplitudes obtained by solving the CC equations are related to the diffraction probabilities or intensities. These intensities are for a zero surface temperature and, in order to compare with the experimental intensities, a Debye–Waller factor is taken into account to obtain theoretical intensities at a given surface temperature.

3.5. Elastic diffraction channels

As inferred from equation (11), in the CC formalism a diffraction channel is represented and governed by an effective potential of the form $V_{\mathbf{0}}(z)+(\mathbf{K}_\mathrm{i}+\mathbf{G})^2$, where the second contribution to the bare potential can be interpreted as the asymptotic energy of the **G** reciprocal lattice vector [23, 27]. Each effective potential has a discrete spectrum as well as a continuum one. Continuum (or diffracted) wavefunctions are usually expressed as $|\mathbf{K}_\mathrm{i} + \mathbf{G}, \mathbf{k}^2_{\mathbf{G},z}\rangle$ and discrete ones as $|\mathbf{K}_\mathrm{i} + \mathbf{G}, v\rangle$, where v is the quantum number associated with the bound states formed between the He atoms and the surface, though in general both are labelled as $\Psi_{\mathbf{G}}(z)$ (see equation (10)). Thus, for the specular channel, one has $|\mathbf{K}_\mathrm{i}, \mathbf{k}^2_z\rangle$. Though one always assumes that kinetic energies are positive quantities, due to the contribution mentioned above, negative effective kinetic energies can also be defined in scattering problems. These energies correspond to closed channels which are not accessible. They have to be taken into account when solving the CC equations in order to get the right numerical convergence. Accordingly, depending on the sign of the kinetic energy, two different types of diffraction channels can be distinguished. If $\mathbf{k}^2_{\mathbf{G},z} > 0$, one has open or energetically accessible diffraction channels. Whereas, if $\mathbf{k}^2_{\mathbf{G},z} < 0$, one has closed or energetically forbidden channels. The specular channel, $\mathbf{G} = \mathbf{0}$, is the only one that is always open, and corresponds to $\theta_\mathrm{f} = \theta_\mathrm{i}$. According to equation (12), the asymptotic energies depend on the lattice constants, the incidence energy, and the incidence polar and azimuthal angles. Therefore, for each scattering geometry, the diffraction channels will display different asymptotic energies, and the relative arrangement of such channels will be quite different each time. In this sense, one speaks about *moving thresholds* [24, 27] in contrast to other types of multichannel scattering described in nuclear, atomic, or molecular physics, where thresholds are fixed.

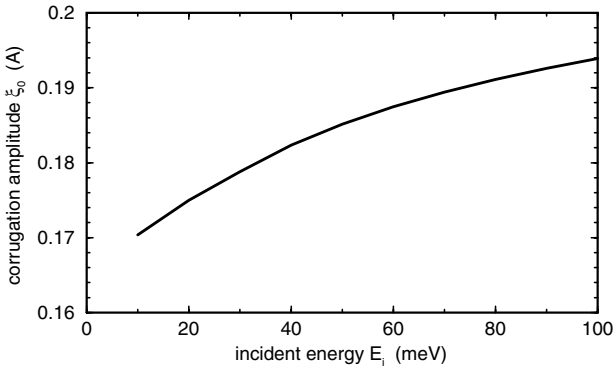

Figure 2. Corrugation amplitude ξ_0 as a function of the incident energy E_i from DFT calculations.

4. Results and discussion

4.1. Eikonal results

In the next step, the eikonal analysis of the corrugation amplitude has been refined by using the energy-dependent effective corrugation function equation (7) instead of equation (6). It is observed that, for a well depth of $D = 12.5$ meV and incident energy of 26.61 meV, the corrugation amplitude has to be slightly increased to $\xi_0 = 0.18$ Å in order to obtain better agreement of the calculated diffraction amplitudes with experiment (around 5–8% of error). However, when the surface is strongly corrugated and, therefore, the number of closed and open diffraction channels is important, large discrepancies have been reported for different systems [25, 31].

4.2. Analysis of the corrugation by DFT

As an alternative pathway to the eikonal analysis of experimental data, DFT calculations were performed to determine the corrugation amplitude of the MgO(001) surface which is experienced by He atoms in a diffraction experiment. The computations were performed using the mixed-basis pseudopotential (MBPP) code [33], employing the PBE functional [34] together with norm-conserving pseudopotentials and a mixed basis set of plane waves (with an energy cutoff of 20 Ryd) and localized atomic orbitals. The MgO surface was represented by periodically repeated slabs consisting of five MgO layers and a (2×2) surface unit cell. The Brillouin-zone integrations were carried out with $4 \times 4 \times 1$ Monkhorst–Pack k-point meshes. The MgO surface was fully relaxed by minimizing the atomic forces. The surface is very rigid and only a small inward movement of the Mg ions is observed, leading to a height difference between the Mg and O ions of 0.05 Å. Thus, the geometric surface corrugation amplitude of the atomic positions amounts only to 0.025 Å.

While DFT calculations employing common LDA or GGA functionals are not suitable to determine the attractive part of the He–MgO interaction, since these functionals (including PBE) insufficiently describe van-der-Waals forces, we can, however, expect reliable results for the repulsive part of the interaction potential. This repulsive part has been determined by using a single He atom approaching the MgO slab at different lateral positions above the surface and calculating the repulsion energy. From this energy map, equipotential energy surfaces are constructed which describe the classical turning points for He atoms with an incidence energy of E_i, thus representing effective corrugation functions as introduced in section 3.3. The shape of these calculated effective corrugation functions is almost indistinguishable from the cosine behaviour of equation (6). The corrugation amplitude ξ_0 as function of the incident energy E_i is

plotted in figure 2. It increases from 0.17 to 0.19 Å in the relevant energy range of 10–80 meV. This is in very good agreement with the result of $\xi_0 = 0.18$ Å of the previous eikonal analysis at 26.61 meV. Thus, in the following CC calculation this value has been used for the corrugation amplitude.

4.3. Analysis of kinematics

Prior to any CC calculation we carry out a kinematic analysis, in order to find the channels that need to be included to obtain numerical convergence for integration.

The square of the perpendicular component of the final momentum ('kinetic energy') of several diffraction channels is plotted versus the incidence energy, the polar angle, and the azimuthal angle in the top, central, and bottom panels of figure 3, respectively. The horizontal solid black line at zero energy indicates, for each incidence energy, which channels are open or closed, depending on whether they are above or below it, respectively. Moreover, in this way *threshold resonances* (TR) can be easily identified, which are the points at which an open channel becomes closed or vice versa. These plots are also convenient for finding resonances (which is not the scope of this work), if the bound levels supported by $V_{\mathbf{0}}(z)$ are also displayed (black dashed lines). Such resonances, the so-called *selective adsorption resonances* (SAR) [27], are found by searching for the crosses of these levels with the closed channels.

In the top panel of figure 3 there are results for an azimuthal angle of 0° and a polar angle of 62.3°. As can be seen, the specular channel is always open (positive kinetic energy), whereas the negative diffraction channels are also open in a very broad energy region. The first closed channel is that corresponding to (1, 1). At very small incidence energies, several crossings or degeneracies of different diffraction channels are also apparent. As expected from the experiment, the $(-1, -1)$ channel is open and degenerate with the $(-2, -2)$ channel at a given incident energy. They seem to be the same channel at this energy value. However, the coupling coefficients will break the degeneracy between both channels in the CC calculations. A similar behaviour is observed in the central panel of figure 3, for an incidence energy of 26.61 meV and an azimuthal angle of 0°. Now the regularity in the crossings for a fixed angle or a fixed energy (in this sense, one thus speaks of a *double* regularity) is more striking. For the (1, 1) channel there is a TR at a polar angle of 42°. This explains why one observes this peak at $\theta_i = 27.87°$ in the experiment. At $\theta_i = 62.3°$ there is a degeneracy in energy between the (1, 1) and (2, 2) channels. Finally, in the bottom panel of figure 3 there is a similar representation to the previous ones, this time as a function of the azimuthal angle, with an incidence energy of 26.61 meV and a polar angle of 62.30°. One can see that for $\phi_i = 0°$ (which happens in our experiment) the $(-1, -1)$ and $(0, 0)$ channels are just opened, as expected from the experimental results. In this case, there is a degeneracy between the $(-1, -1)$ and $(-2, -2)$ channels.

The number of **G**-channels involved depends strongly on the surface corrugation or strength of the Fourier coefficients of the interaction potential, $V_{\mathbf{G}-\mathbf{G}'}(z)$, which are responsible for the coupling among different channels. These Fourier coefficients are usually repulsive and increase very rapidly for small z. For all $V_{\mathbf{G}}(z)$ with $\mathbf{G} \neq \mathbf{0}$, the effective range is short and decreases with $|\mathbf{G}|$. The computer time scales with N^3, with N being the total number of (open and closed) diffraction channels involved in a scattering geometry.

4.4. Calculations of diffraction intensities

After this kinematic analysis, in figure 4 our CC results (triangles) are plotted together with He diffraction peaks [21] at $E_i = 26.61$ meV (panel (a)) and $E_i = 60.46$ meV (panel (b)) at a surface temperature of 300 K. Eikonal results are not plotted because, at the resolution of

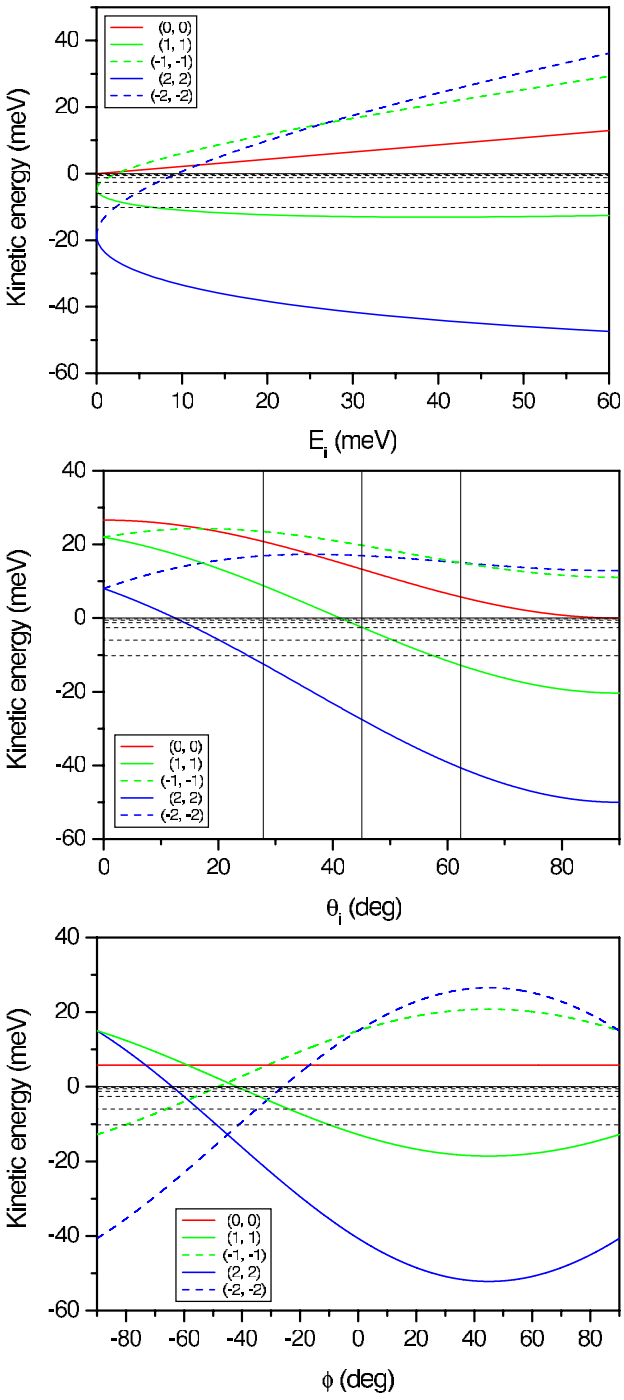

Figure 3. Top: z-kinetic energies for He–MgO(001) scattering as a function of the incidence energy, keeping constant the polar and azimuthal angles at 62.3° and 0°, respectively. Centre: z-kinetic energies for He–Mg(001) scattering as a function of the incidence polar angle, keeping constant the incidence energy and the azimuthal angle at 26.61 meV and 0°, respectively. The three vertical lines correspond to the three experimental polar angles (see figure 4). Bottom: z-kinetic energies for He–MgO(001) scattering as a function of the azimuthal angle, keeping constant the incidence energy and polar angle at 26.61 meV and 62.3°, respectively. In the three figures, the pairs of integer numbers label two diffraction channels: the negative channel goes upwards while the positive channel goes downwards. Black dashed lines represent the bound energy levels supported by $V_{\mathbf{0}}(z)$.

such a figure, there is no appreciable difference with experimental and CC results. The Debye–Waller factor has been included in the CC points by using a Debye temperature of 495 K (the application of the Debye–Waller factor in HAS results has been discussed elsewhere [32]). The

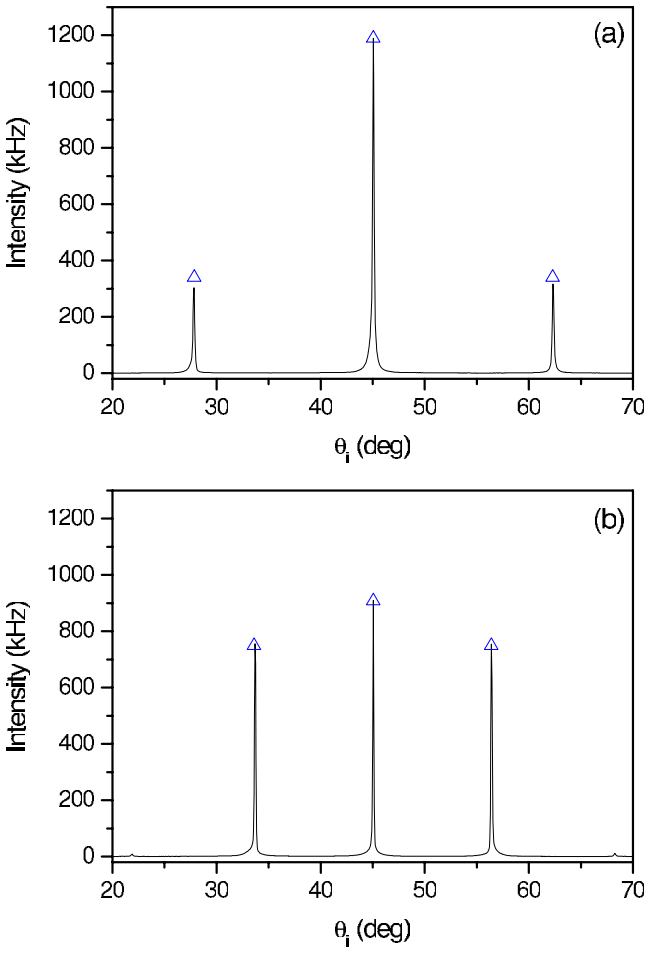

Figure 4. Diffraction patterns as a function of the incident angle for the clean MgO(100) surface measured along the ⟨100⟩ direction for: (a) $E_i = 26.61$ meV and (b) $E_i = 60.46$ meV and at a surface temperature of 300 K. The triangles show our CC results.

corresponding corrugation amplitudes have been chosen from the DFT calculations: 0.18 Å and 0.186 Å, respectively. For the higher incident energy, the stiffness parameter has been 1.02 $Å^{-1}$, which is slightly different to the previous value of 1.0 $Å^{-1}$. The agreement with the experiment is very good, with a deviation of 0.1%. However, it should be noted that in this work the maximum peak intensities have been used, whereas in the simple eikonal analysis of [21] peak areas have been fitted and slightly different corrugation amplitudes for the ⟨110⟩ direction were obtained than for the ⟨100⟩ direction. In future work a more detailed comparison will be tackled. Thus, we have shown that the potentials derived in a refined eikonal analysis are indeed good enough according to our DFT calculations.

5. Conclusions

In the present paper we have shown that the experimental diffraction patterns of He–MgO can be correctly reproduced by CC calculations when DFT calculations are used to obtain

corrugation functions. For one incident energy (the lowest one), we have obtained the same corrugation amplitude by a fitting procedure using an effective corrugation function together with the CC method. This procedure can be quite cumbersome for dense diffraction patterns, since the number of calculations and diffraction channels are very high. In the case of MgO, the eikonal approximation with effective corrugation function gives good results and, therefore, can be used to extract potential information if electronic densities are not known or difficult to obtain by first principles. As shown here, DFT is suitable for giving very accurate information on the surface corrugation without any assumptions concerning its shape or energy dependence and, consequently, modelling of He diffraction from more complicated surfaces becomes feasible. Additional information from DFT calculations such as the stiffness parameter should also be extracted, since reliable results for the repulsive part of the interaction potential are easily attainable.

References

[1] Henrich V E and Cox P A 1996 *The Surface Science of Metal Oxides* (Cambridge: Cambridge University Press)
[2] Freund H-J, Kuhlenbeck H and Staemmler V 1996 *Rep. Prog. Phys.* **59** 283
[3] Diebold U 2003 *Surf. Sci. Rep.* **48** 53
[4] Noguera C 2000 *J. Phys.: Condens. Matter* **12** R367
[5] Campbell C T 1997 *Surf. Sci. Rep.* **27** 1
[6] Traeger F 2006 *Chem. Phys. Chem.* **7** 1006
[7] Brusdeylins G, Doak R B, Skofronick J G and Toennies J P 1983 *Surf. Sci.* **128** 191
[8] Mahgerefteh M, Jung D R and Frankl D R 1989 *Phys. Rev.* B **39** 3900
[9] Jung D R, Mahgerefteh M and Frankl D R 1989 *Phys. Rev.* B **39** 11164
[10] Cantini P and Cevasco E 1984 *Surf. Sci.* **148** 37
[11] Cui J, Jung D R and Frankl D R 1990 *Phys. Rev.* B **42** 9701
[12] Jung D R, Cui J and Frankl D R 1991 *J. Vac. Sci. Technol.* **A9** 1589
[13] Rieder K H 1982 *Surf. Sci.* **118** 57
[14] Cantini P, Tatarek R and Felcher G P 1979 *Phys. Rev.* B **19** 1161
[15] Witte G, Senet P and Toennies J P 1998 *Phys. Rev.* B **58** 13264
[16] Toennies J P 1993 *J. Phys.: Condens. Matter* **5** A25
[17] Hulpke E (ed) 1992 *Helium Atom Scattering from Surfaces* (*Springer Series in Surface Science* vol 27) (Berlin: Springer) and references therein
[18] Farías D and Rieder K H 1998 *Rep. Prog. Phys.* **61** 1575 and references therein
[19] Poelsema B and Comsa G 1989 *Scattering of Thermal Energy Atoms from Disordered Surfaces* (*Springer Tracts in Modern Physics*) (Berlin: Springer)
[20] Garibaldi U, Levi A C, Spadacini R and Tommei G E 1975 *Surf. Sci.* **48** 649
[21] Benedek G, Brusdeylins G, Senz V, Skofronick J G, Toennies J P, Traeger F and Vollmer R 2001 *Phys. Rev.* B **64** 125421
[22] Eichenauer D, Harten U, Toennies J P and Celli V 1987 *J. Chem. Phys.* **86** 3693
[23] Hernández M, Roncero O, Miret-Artés S, Villarreal P and Delgado-Barrio G 1989 *J. Chem. Phys.* **90** 3823
[24] Hernández M, Miret-Artés S, Villarreal P and Delgado-Barrio G 1991 *Surf. Sci.* **251/252** 369
Hernández M, Miret-Artés S, Villarreal P and Delgado-Barrio G 1992 *Surf. Sci.* **274** 21
[25] Miret-Artés S, Toennies J P and Witte G 1996 *Phys. Rev.* B **54** 5881
[26] Guantes R, Sanz A S, Margalef-Roig J and Miret-Artés S 2004 *Surf. Sci. Rep.* **53** 199
[27] Sanz A S and Miret-Artés S 2007 *Phys. Rep.* at press
[28] Hernández M I, Campos-Martinez J, Miret-Artés S and Coalson R D 1994 *Phys. Rev.* B **49** 8300
[29] Toennies J P and Vollmer R 1991 *Phys. Rev.* B **44** 9833
[30] Armand G and Manson J R 1982 *Surf. Sci.* **119** L299
[31] Siber A and Gumhalter B 2003 *Surf. Sci.* **529** L269
[32] Siber A and Gumhalter B 2003 *Phys. Rev. Lett.* **90** 126103
[33] Meyer B, Lechermann F, Elsässer C and Fähnle M *Fortran90 Program for Mixed-Basis Pseudopotential Calculations for Crystals* Max-Planck-Institut für Metallforschung, Stuttgart
[34] Perdew J P, Burke K and Ernzerhof M 1996 *Phys. Rev. Lett.* **77** 3865
Perdew J P, Burke K and Ernzerhof M 1997 *Phys. Rev. Lett.* **78** 1396 (erratum)